ADVANCED ELECTRONIC MATERIALS
www.advelectronicmat.de

Efficient Orange–Red Delayed Fluorescence Organic Light-Emitting Diodes with External Quantum Efficiency over 26%

Feng-Ming Xie, Ping Wu, Shi-Jie Zou, Yan-Qing Li, Tao Cheng, Miao Xie, Jian-Xin Tang, and Xin Zhao**

Highly efficient orange–red/red thermally activated delayed fluorescence (TADF) materials have been rarely reported due to the restriction of their molecular design in the energy gap law. An effective strategy is to use large rigid planar units and strong intramolecular charge transfer for synthesizing efficient long-wavelength TADF materials. Three novel orange–red to red TADF materials are obtained using a large rigid planar dibenzo[a,c]phenazine (BP) acceptor core and different numbers of strong electron-donating phenoxazine (PXZ) moieties, namely 1PXZ-BP, 2PXZ-BP, and 3PXZ-BP. The increase in the number of PXZ units red-shifts the emission from 602 to 682 nm in solution. Moreover, these emitters are endowed with high electroluminescence performance due to small singlet–triplet energy difference (ΔE_{ST}), fast radiative rate, and high photoluminescence quantum yields. 1PXZ-BP-based orange–red organic light-emitting diodes (OLEDs) achieve an excellent external quantum efficiency of 26.3%, which is one of the highest efficiencies reported for orange–red TADF OLEDs.

1. Introduction

Organic light-emitting diodes (OLEDs) have become a leading display technology due to their steadily improved efficiency and unique features such as fascinating flexibility, lightweight, no turn-on delay, superior color gamut, and wide viewing angle.[1–6] The key electroluminescent (EL) materials in OELDs are traditional fluorescent and phosphorescent materials. Fluorescent materials are inefficient with the maximum internal quantum efficiency (IQE) of only 25%, while phosphorescent materials require the use of rare and expensive noble metals (such as iridium and platinum) although its IQE can reach 100% in theory.[6–9] As an alternative, third-generation EL materials of thermally activated delayed fluorescence (TADF) with low-cost pure organic molecular structures have been attracting much attention in recent years since they can harvest both singlet and triplet excitons through reverse intersystem crossing (RISC) process to reach the theoretical IQE close to 100%.[9,10] To date, rapid progress of blue and green TADF materials has been made,[7,11] whereas there have been rare reports on high-efficiency orange-red TADF OLEDs.[12–14] Therefore, much space is still left for improvement in orange-red TADF emitters to make up for their backward.

For the design of efficient TADF emitters, one key factor is to minimize the energy difference (ΔE_{ST}) between the lowest singlet (S_1) and triplet (T_1) states, and thus improve the up-conversion rate (k_{RISC}) from T_1 to S_1 and potentially increase the IQE of a device.[4,15,16] So far, the molecular design principles of TADF emitters generally have three species: twisted intramolecular charge transfer (TICT), through-space charge transfer (TSCT), and multi-resonance induced TADF (MR-TADF).[17] The most common molecular design strategy of TADF emitters is using a pre-twisted donor–acceptor (D–A) type structure with twisted intramolecular charge transfer (TICT) transition from the highest occupied molecule orbital (HOMO) to the lowest unoccupied molecule orbital (LUMO), which can significantly reduce the ΔE_{ST} values.[10,18–20] For the design of efficient TADF molecules, another important factor is the molecular rigidity. Molecular rigidity can be obtained by a large dihedral angle in a twisted donor-acceptor structure, which is favorable for the RISC process.[21] However, the development of higher-efficiency TADF emitters and devices remain challenges owing to the intricacies of the TADF mechanism.[21] One of the major challenges in achieving highly efficient orange-red TADF emitters is to simultaneously realize small ΔE_{ST} (less than 0.3 eV), fast radiative decay rate constant (k_r), high photoluminescence quantum yields (PLQYs), larger molecular rigidity, and strong TICT through the rational molecular design.[17,22–25] Moreover, it is difficult to enhance the

Dr. F.-M. Xie, P. Wu, Prof. X. Zhao
College of Chemistry, Biology and Material Engineering
Suzhou University of Science and Technology
Suzhou, Jiangsu 215009, China
E-mail: zhaoxin_sz@usts.edu.cn
Dr. S.-J. Zou, Prof. Y.-Q. Li, Prof. T. Cheng, Dr. M. Xie, Prof. J.-X. Tang
Jiangsu Key Laboratory for Carbon-Based Functional Materials & Devices
Institute of Functional Nano & Soft Materials
Soochow University
Suzhou, Jiangsu 215123, China
E-mail: jxtang@suda.edu.cn
The ORCID identification number(s) for the author(s) of this article can be found under https://doi.org/10.1002/aelm.201900843.

DOI: 10.1002/aelm.201900843

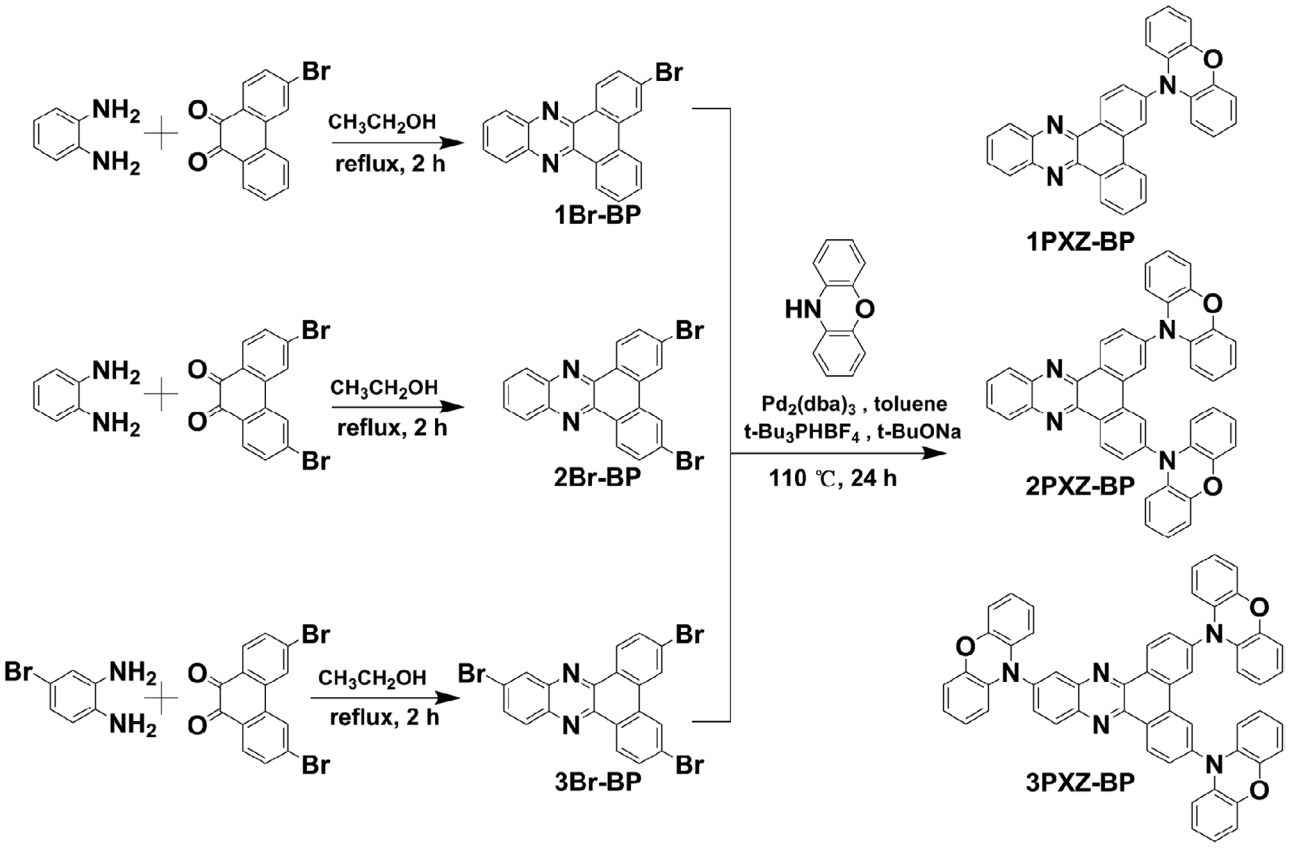

Scheme 1. Synthetic routes of the TADF emitters of 1PXZ-BP, 2PXZ-BP, and 3PXZ-BP, respectively.

PLQYs for orange-red/red TADF materials, since this PLQYs value can decrease with respect to the increase in emission wavelength in view of energy-gap law.[25]

In this work, we design and synthesize high-efficiency orange-red/red TADF materials based on large rigid planar dibenzo[a,c]phenazine (BP) acceptor core and different numbers of phenoxazine (PXZ) donors (**Scheme 1**). The BP unit is selected as an excellent large rigid coplanar skeleton unit for building long-wavelength TADF molecules,[14] while PXZ shows the strong electron-donating ability and shallow HOMO level as compared to other donor units like 9,9-dimethylacridan (DMAC) (Figure S1, Supporting Information).[26] A series of orange-red/red emitters, *x*PXZ-BP (x = 1, 2, 3), have been constructed by red-shifting the emission wavelength with an increase in the number of PXZ unit. All three compounds show long-wavelength emission over 600 nm, notably, 3PXZ-BP exhibits a deep-red emission at around 682 nm in toluene solution. The OLEDs based on the three emitters show excellent electroluminescence performance. Red device based on 3PXZ-BP exhibits a maximum external quantum efficiency (EQE) of 7.1% with a EL peak at 634 nm. Orange-red device based on 2PXZ-BP obtains a maximum EQE of 19.2% with a EL peak at 606 nm. Especially, because of the fastest k_r, highest PLQY, and small ΔE_{ST} among *x*PXZ-BP (x = 1, 2, 3), 1PXZ-BP-based orange-red OLEDs achieve the highest EQE of 26.3%, which is one of the highest efficiencies reported for orange-red TADF OLEDs.

2. Results and Discussion

2.1. Theoretical Calculations

Generally, a widely used strategy to obtain small ΔE_{ST} in D–A-type TADF molecules is to increase the separation of frontier molecular orbitals (FMOs), which can be achieved by using the steric effect with a large dihedral angle between D and A units. Density functional theory (DFT) and time-dependent DFT calculations were carried out by Gaussian 09 program with B3LYP/6-31G(d) basis sets to investigate the FMOs, HOMO/LUMO levels, ground states, and excited states properties of BP derivatives (i.e., 1PXZ-BP, 2PXZ-BP, and 3PXZ-BP) in toluene solution.[2,5] As shown in **Figure 1**, all the dihedral angles between PXZ donor and BP acceptor are above 80° for three pre-twisted molecules in the optimized geometries. Moreover, the FMOs of all three compounds are almost completely separated, in which the LUMO levels are localized at the BP unit but the HOMO levels are mainly localized at the electron-donating PXZ moiety with a slight extent on the adjacent benzene ring. However, it is noted that the HOMO level of 3PXZ-BP is not localized at the PXZ unit of 11-position. The PXZ group introduced at 11-position will cause the actual transition process from HOMO-2 to LUMO (Figure S2a, Supporting Information), which usually requires much energy. Moreover, the increase in the number of PXZ units results in a decrease in the S_1/T_1 levels (Figure S2b, Supporting Information). The calculated

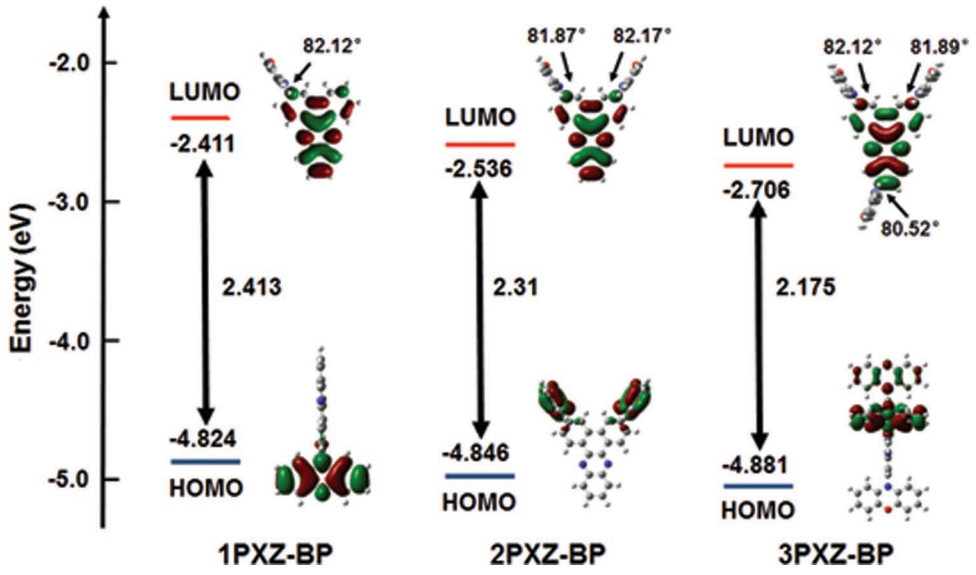

Figure 1. Energy levels and FMOs with the optimized structures of 1PXZ-BP, 2PXZ-BP, and 3PXZ-BP, respectively.

S_1/T_1 levels show the values of 2.0123/2.0090 eV, 1.9139/1.9106 eV, and 1.7216/1.7104 eV for 1PXZ-BP, 2PXZ-BP, and 3PXZ-BP, respectively, corresponding to the ΔE_{ST} of 3.3, 3.3, and 11.2 meV. According to the DFT calculations, the rather small ΔE_{ST} values and well-separated HOMO-LUMO level distributions may contribute to the effective RISC processes from T_1 to S_1, leading to high PLQYs for 1PXZ-BP, 2PXZ-BP, and 3PXZ-BP.

2.2. Photophysical Properties

1PXZ-BP, 2PXZ-BP, and 3PXZ-BP were synthesized through a simple two-step reaction (Scheme 1). After purification by silica gel column chromatography, these molecules were certified by ^{1}H NMR, ^{13}C NMR, and high-resolution mass spectrometry (Figures S3–S11, Supporting Information). Cyclic voltammetry (CV) curves of BP derivatives reveal the reversible oxidation potentials (Figures S12 and S13, Supporting Information). The HOMO/LUMO levels of these compounds were experimentally estimated from the first oxidation potentials and optical energy gap (E_g). As summarized in **Table 1**, the HOMO/LUMO levels of 1PXZ-BP, 2PXZ-BP, and 3PXZ-BP are −5.03/−2.56 eV, −5.05/−2.63 eV, and −5.02/−2.90 eV, respectively, which are in good agreement with the theoretical calculation results (Figure 1). In addition, these compounds exhibit high decomposition temperatures (T_d) in the range of 391–401 °C (Figure S14, Supporting Information).

As depicted in **Figure 2**a, *x*PXZ-BP (x = 1, 2, 3) exhibit the similar absorption spectra in diluted toluene solutions (1×10^{-5} M), all of them show two major absorption band, the high energy band around 280 nm can be originated from the π–π^* transition of the conjugated skeleton. The absorption bands at 410–600 nm can be ascribed to the ICT from the electron donor PXZ to the electron acceptor BP, which indicate all three compounds possess strong ICT effect. Compared to 1PXZ-BP and 2PXZ-BP, 3PXZ-BP has more stronger ICT effect due to its wider lowest-energy absorption band at 420–600 nm. It is found in Figure 2a that these compounds show the fluorescence in a wide range from orange (602 nm) to dark-red (682 nm) in toluene by increasing the number of PXZ units and strong ICT effects. According to the onset wavelengths of fluorescence and phosphorescence spectra measured in toluene at 77 K (Figure 2b), the ΔE_{ST} values of 1PXZ-BP, 2PXZ-BP, and 3PXZ-BP are estimated to be 0.25, 0.10, and 0.03 eV, respectively. The smallest ΔE_{ST} for 3PXZ-BP implies that it may possess the fastest RISC process from T_1 to S_1. These results provide the experimental evidence of the possibility of tuning the S_1 and T_1 states with respect to the increase in the number of

Table 1. Summary of photophysical, electrochemical, and thermal properties of 1PXZ-BP, 2PXZ-BP, and 3PXZ-BP.

Emitter	$\lambda_{Fl.}$[a] (RT) [nm]	λ_{Ph}[b] (77 K) [nm]	ΔE_{ST}[c] [eV]	FWHM[d] (RT) [nm]	PLQY[e] (neat/doped) [%]	T_d[f] [°C]	E_g[g] [eV]	HOMO/LUMO[h] [eV]
1PXZ-BP	602	550	0.25	101	40/73	391	2.47	−5.03/−2.56
2PXZ-BP	625	563	0.10	101	37/63	397	2.42	−5.05/−2.63
3PXZ-BP	682	620	0.03	110	11/22	401	2.12	−5.02/−2.90

[a]Fluorescence peak (λ_{Fl}) at room temperature in toluene (1.0×10^{-5} M); [b]Phosphorescence peak (λ_{Ph}) at 77 K in toluene; [c]ΔE_{ST} determined from the energy difference between λ_{Fl} and λ_{Ph}; [d]The full-width at half maximum (FWHM) of fluorescence at room temperature; [e]Absolute PLQY measured for neat films and doped films at room temperature; [f]Decomposition temperature (T_d) with 5% weight loss; [g]E_g was estimated from the absorption onset in toluene; [h]HOMO levels were determined from the oxidation potential onset of cyclic voltammetry with $E_{HOMO} = -e(E^{onset}_{ox} + 4.8)$, and $E_{LUMO} = E_g + E_{HOMO}$.

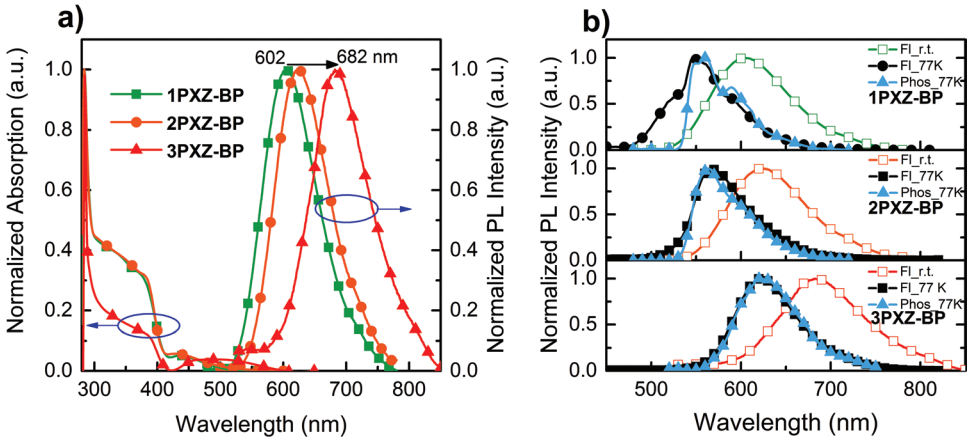

Figure 2. a) Normalized UV–vis absorption and fluorescence spectra, b) normalized PL spectra at room temperature and 77 K of 1PXZ-BP, 2PXZ-BP, and 3PXZ-BP in toluene, respectively.

PXZ units. Absolute PLQYs of three BP derivatives were measured in neat and doped films in nitrogen atmosphere at room temperature, where 4,4'-di(9H-carbazol-9-yl)-1,1'-biphenyl (CBP) was used as a host for the doping of BP derivatives.[27] As summarized in Table 1, the relatively high PLQYs of 73%, 63%, and 22% were obtained for 1PXZ-BP, 2PXZ-BP, and 3PXZ-BP doped in CBP, respectively. In contrast, the corresponding values were obviously reduced to 40%, 37%, and 11% in the neat films (Table 1), which can be ascribed to the suppression of up-conversion and radiative decay process for TADF molecules under the concentrated condition.[28]

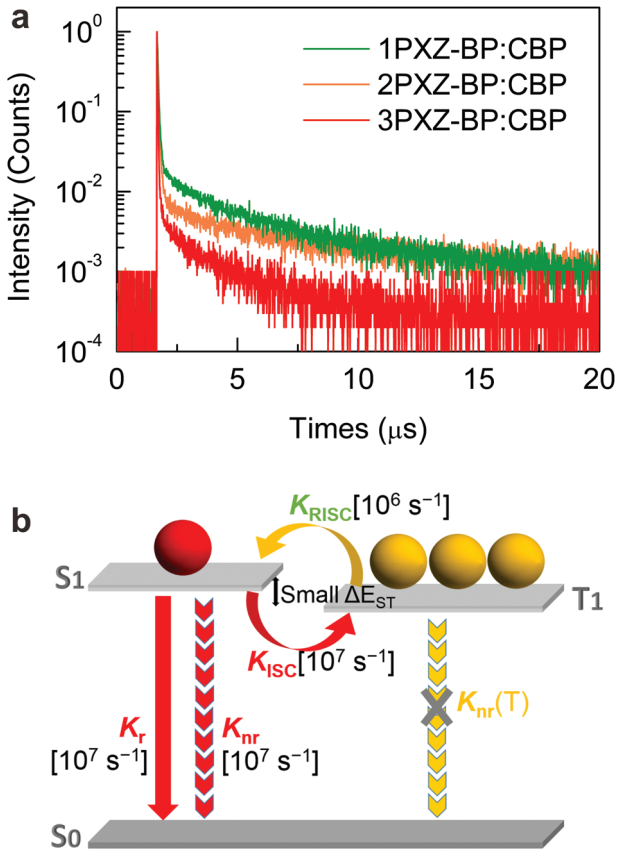

Figure 3. a) Room-temperature transient PL decay curves of 1PXZ-BP, 2PXZ-BP, and 3PXZ-BP. b) Schematic of the RISC process in BP derivatives.

Figure 3a displays the transient photoluminescence (PL) decay curves of BP derivatives doped into the host of CBP, and the temperature dependence of transient PL decays were also compared in **Figure 4**. These spectra present the obvious delayed fluorescence features. As shown in Figure 3a, these compounds exhibit notable differences. Particularly, the delayed fluorescence lifetime (τ_d) remarkably decreases with respect to the addition of PXZ units, leading to a faster prompt fluorescence lifetime (τ_p). As summarized in Table S1, Supporting Information, the τ_p/τ_d are estimated to be 47 ns/4.8 μs, 65 ns/4.3 μs, and 28 ns/2.0 μs for 1PXZ-BP, 2PXZ-BP, and 3PXZ-BP, respectively. Enhanced RISC was also observed previously for a green-emitting molecule with three donors and one acceptor unit.[22] As schematically illustrated in Figure 3b, the similar RISC process can take place in BP derivatives with different numbers of PXZ units. The short delayed fluorescence lifetimes between 2 to 5 μs indicate that T_1 state excitons can rapidly convert to S_1 state through RISC and thus reduce triplet-triplet-annihilation (TTA).[27,29] Moreover, the reduction of τ_d is accompanied with a substantial increase in the RISC rate constant (k_{RISC}) from 1PXZ-BP to 3PXZ-BP. However, the kr for singlet excitons is reduced from 0.64×10^7 to 0.29×10^7 s^{-1} from 1PXZ-BP to 3PXZ-BP, and at the same time the nonradiative decay rate constant (knr) of 3PXZ-BP is almost four times larger than that of 1PXZ-BP (Table S1, Supporting Information). These results can account for the reason of the decrease in PLQYs from 1PXZ-BP to 3PXZ-BP as shown in Table 1.

2.3. Device Performance

To evaluate the EL performane of these TADF materials, OLEDs with BP derivatives as emitters were fabricated in a device structure of ITO/HAT-CN (10 nm)/TAPC (45 nm)/TADF:CBP (15 nm, 7 wt%)/B3PYMPM (45 nm)/Liq (1 nm)/Al (100 nm) (see the chemical structures of organic materials and fabrication details

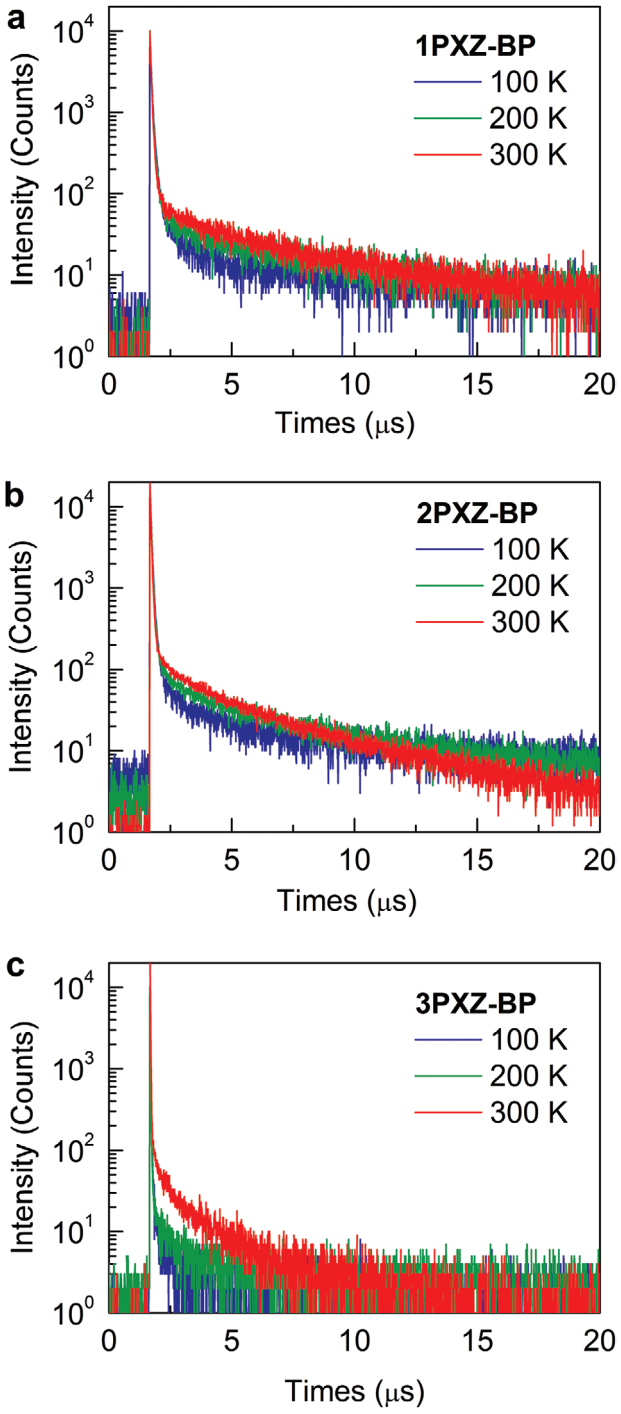

Figure 4. Temperature-dependent transient PL decay curves of a) 1PXZ-BP, b) 2PXZ-BP, and c) 3PXZ-BP (7 wt%) doped in CBP.

in Experimental Section). **Figure 5**a displays the schematic diagram of energy levels of the multilayered device structure, in which HOMO and LUMO levels of three BP derivatives match well with the CBP host for effectively capturing the holes and electrons. Figure 5b shows the EL spectra and emission colors of three TADF OLEDs. The orange-red OLEDs based on 1PXZ-BP and 2PXZ-BP exhibit the orange-red colors with the EL peak (λ_{EL}) at 590 and 606 nm together with a full-width at half-maximum (FWHM) of 106 nm. The corresponding CIE color coordinates are (0.52, 0.46) and (0.57, 0.42) for 1PXZ-BP and 2PXZ-BP. On the contrary, pure-red emission is achieved for 3PXZ-BP-based OLED, showing a λ_{EL} at 634 nm with a FWHM of 111 nm and the CIE color coordinates of (0.62, 0.37). Obviously, the EL peak positions of three devices were almost identical to the PL peaks of *x*PXZ-BP-doped CBP films, but blue-shifted as compared to the neat *x*PXZ-BP films as listed in Table S2, Supporting Information. Figure 5c plots the current density–voltage–luminance (J–V–L) curves, and the key device performances are summarized in **Table 2**. It is apparent that all three OLEDs exhibit the almost identical electrical properties with low turn-on voltages (V_{on}), which are 2.6, 2.6, and 2.5 V for 1PXZ-BP, 2PXZ-BP, and 3PXZ-BP, respectively. Correspondingly, the maximum brightness (L_{max}) of three OLEDs are 5082 cd m^{-2}, 4818 cd m^{-2}, and 1269 cd m^{-2}, respectively. Figure 5d shows the EQE-luminance characteristics of three TADF OLEDs. The 1PXZ-BP-based device shows the maximum EQE of 26.3%, power efficiency (PE) of 57.1 lm W^{-1}, and current efficiency (CE) of 47.2 cd A^{-1}, respectively (Figure S15, Supporting Information), which may arise from the highest PLQY, fastest k_r value, and small ΔE_{ST}. To date, a peak EQE of 26.3% is one of the highest efficiencies reported in the literatures for orange-red TADF OLEDs. Meanwhile, the maximum EQE values are 19.2% and 7.1% for orange-red/red TADF OLEDs employing 2PXZ-BP and 3PXZ-BP, respectively, which are competitive to those of orange-red and red TADF emitters.[22,30–35] However, we find that the efficiency roll-off of three emitters (xPXZ-BP) are all higher, we speculate that the main reason might be inferior charge balance of the devices.[7] And this issue remains to be further explored. To understanding such high EQE of our devices, the molecular structure of xPXZ-BP was obtained by simulated calculation using density functional theory (DFT) (Figure S16, Supporting Information). Finding the three emitters xPXZ-BP all possess satisfying plane structure, which is beneficial to generate horizontally orientated dipoles, and increase the light out-coupling efficiency(η_{out}) of the OLEDs.[7,11,36] So such high EQE might be attributed to the favorable dipole orientation of our emitters due to their plane structure(higher η_{out}), small ΔE_{ST}, relatively high PLQY, fast kr, and short delayed fluorescence exciton lifetime.

3. Conclusion

In summary, a series of D–A-type orange-red/red TADF materials (namely 1PXZ-BP, 2PXZ-BP, and 3PXZ-BP) have been designed and synthesized by combining the large rigid coplanar BP acceptor and different number of strong electron-donating PXZ donors. Rational molecular design not only tunes the emission wavelength effectively from 602 to 682 nm in solution, but also simultaneously endows them small ΔE_{ST}, relatively high PLQYs, fast k_r, and favorable dipole orientation. The orange-red OLED based on 1PXZ-BP and 2PXZ-BP achieve maximum EQE values of 26.3% and 19.2%, respectively, which are competitive to that of previously reported orange-red TADF OLEDs to date. We anticipate that our design concept for highly efficient orange-red/red TADF OLEDs would be favorable to the development of future electroluminescent materials and devices.

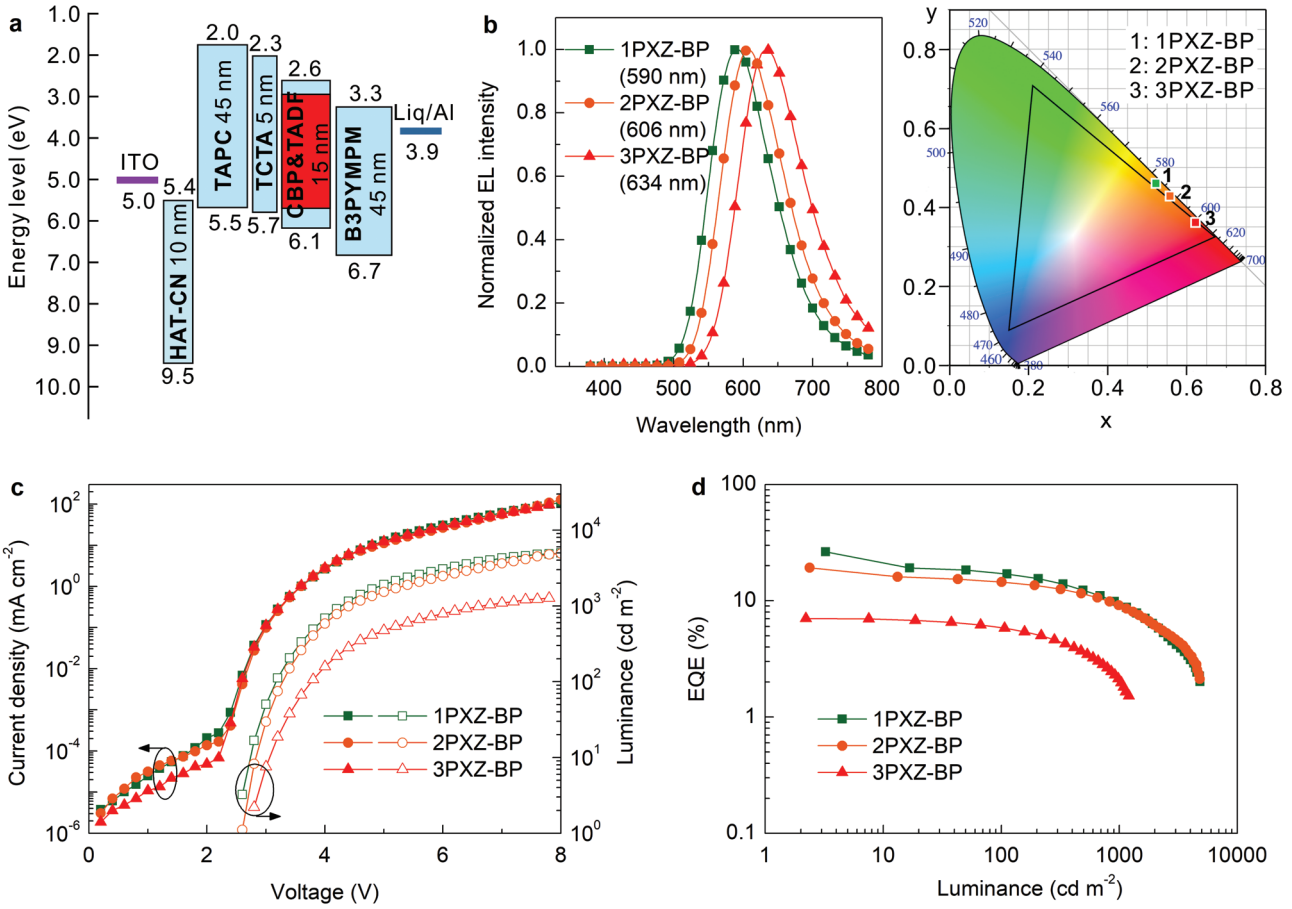

Figure 5. a) Energy level diagram of orange-red/red OLEDs based on different BP derivatives. b) EL spectra and CIE coordinates. c) Current density–voltage–luminance (J–V–L) characteristics. d) EQE as a function of luminance.

4. Experimental Section

Material Synthesis and Device Fabrication: All materials were commercially purchased without further purification. The purity of all solvents is AR. BP intermediates were first synthesized by simple and high-yield reaction. Then, BP and PXZ were linked to synthesize three new compounds by C–N coupling reaction, namely 10-(dibenzo[a,c]phenazin-3-yl)-10H-phenoxazine **(1PXZ-BP)**, 3,6-di(10H-phenoxazin-10-yl)dibenzo[a,c]phenazine **(2PXZ-BP)**, and 10,10′,10″-(dibenzo[a,c]phenazine-3,6,11-triyl)tris(10H-phenoxazine) **(3PXZ-BP)**. Details of the synthesis procedure are shown in **Scheme 1** and Supporting Information. Their chemical structures were verified by ^{1}H NMR, ^{13}C NMR, and high-resolution mass spectrometry. OLEDs were fabricated on the indium-tin-oxide (ITO) coated glass substrates. The ITO-coated glass substrates were ultrasonically cleaned with acetone, ethanol, and deionized water, and then dried in an oven at 110 °C. After the UV-ozone treatment for 15 min, the ITO-coated glass substrates were transferred into a high-vacuum evaporation chamber (base pressure ≤ 2×10^{-6} mbar) for the deposition of organic materials and metal electrodes with a shadow mask. Here, 2,3,6,7,10,11-hexacyano-1,4,5,8,9,12-hexaazatriphenylene (HAT-CN) was used as a hole-injection layer, 1,1-bis(4-di-p-tolylaminophenyl)cyclohexane (TAPC) was used as a hole-transport layer, 4,4′,4″-tris(*N*-carbazolyl)-triphenylamine (TCTA) was used as an electron/exciton-blocking layer, 4,4′-di(9H-carbazol-9-yl)-1,1′-biphenyl (CBP) was used as the host material, 4,6-bis(3,5-di-3-pyridylphenyl)-2-methylpyrimidine (B3PYMPM) was used as an electron-transport layer, 8-hydroxyquinoline lithium (Liq) was used as electron-injection material, and Al was used as the cathode. The active area was determined to be 0.1 cm^2. Deposition rates were 1–2 Å s^{-1} for organic materials, 0.2 Å s^{-1} for Liq layer, and > 6 Å s^{-1} for Al, respectively.

Instruments and Characterization: ^{1}H NMR and ^{13}C NMR spectra were recorded with Germany Bruker AVANCE Å type NMR

Table 2. Characteristics of TADF OLEDs based on 1PXZ-BP, 2PXZ-BP, and 3PXZ-BP.

Emitter	V_{on}[a)] [V]	L_{max}[b)] [cd m^{-2}]	PE[c)] [lm W^{-1}]	CE[d)] [cd A^{-1}]	EQE[e)] [%]	λ_{EL}[f)] [nm]	FWHM[g)] [nm]	CIE(x, y)
1PXZ-BP	2.6	5082	57.1	47.2	26.3/17.2/9.5	590	106	(0.52, 0.46)
2PXZ-BP	2.6	4818	33.1	27.4	19.2/14.5/9.1	606	106	(0.57, 0.42)
3PXZ-BP	2.5	1269	8.8	7.8	7.1/5.5/1.5	634	111	(0.62, 0.37)

[a)]V_{on}, turn-on voltage; [b)]L_{max}, maximum luminance; [c)]PE, maximum power efficiency; [d)]CE, maximum current efficiency; [e)]EQE, maximum EQE and values at 100 and 1000 cd m^{-2}; [f)]λ_{EL}, EL peak; [g)]FWHM, the full-width at half-maximum of the EL spectra.

Spectrometer in $CDCl_3$ solution. Mass spectra were measured on a GCT Premier type (Electron Bombardment (EI)) high-resolution time-of-flight mass spectrometer (TOF-MS). The UV–vis absorption spectra were recorded with a Lambda 750 UV–vis spectrophotometer. The fluorescence luminescence spectra were measured using a FM-4 type fluorescence spectrophotometer (JY company), French. Low-temperature phosphorescence spectra were measured with a FLS 920 spectrometer (Einburgh Corporation) by using the toluene as a solvent at 77 K. Transient PL spectra were measured using Fluorescence lifetime spectrometer C11367 series (Quantaurus-Tau). PLQYs were obtained by using a C9920-02G type fluorescence spectrophotometer (HAMAMASTU, Japan) with an integrating sphere at room temperature in a nitrogen atmosphere. Cyclic voltammetry (CV) was measured on a RST 3100 electrochemical work station with a platinum disk working electrode, a platinum wire counter electrode, a Ag/AgCl reference electrode, and tetrabutylammonium hexafluorophosphate (0.1 M) as the supporting electrolyte. The cyclic voltammograms were obtained at a scanning rate of 50 mV s^{-1} with an DCM solution. TGA was conducted with a HCT-2 instrument at a heating rate of 10°C min^{-1} in a nitrogen atmosphere. DSC was performed on a Pyris Diamond DSC Thermal Analyzer under a nitrogen flow at a heating rate of 10 °C min^{-1}. Current density–voltage–luminance (J–V–L) characteristics and EL spectra of OLEDs were measured simultaneously with a computer controlled programmable power source (Keithley model 2400) and a luminance meter/spectrometer (PhotoResearch PR670).

Supporting Information

Supporting Information is available from the Wiley Online Library or from the author.

Acknowledgements

This work was financially supported by the National Key R&D Program of China (No. 2016YFB0401002), the National Natural Science Foundation of China (Grant Nos. 61520106012, 61705154, 51873138), Collaborative Innovation Center of Suzhou Nano Science & Technology.

Conflict of Interest

The authors declare no conflict of interest.

Keywords

dibenzo[a,c]phenazine, orange–red emission, organic light-emitting diodes, thermally activated delayed fluorescence

Received: August 6, 2019
Revised: September 30, 2019
Published online:

[1] J. Xue, Q. Liang, R. Wang, J. Hou, W. Li, Q. Peng, Z. Shuai, J. Qiao, *Adv. Mater.* **2019**, *31*, e1808242.
[2] L. Gan, Z. Xu, Z. Wang, B. Li, W. Li, X. Cai, K. Liu, Q. Liang, S. J. Su, *Adv. Funct. Mater.* **2019**, *29*, 1808088.
[3] D. Liu, W. Tian, Y. Feng, X. Zhang, X. Ban, W. Jiang, Y. Sun, *ACS Appl. Mater. Interfaces* **2019**, *11*, 16737.
[4] V. Thangaraji, P. Rajamalli, J. Jayakumar, M. Huang, Y. Chen, C. Cheng, *ACS Appl. Mater. Interfaces* **2019**, *11*, 17128.
[5] W. Zeng, T. Zhou, W. Ning, C. Zhong, J. He, S. Gong, G. Xie, C. Yang, *Adv. Mater.* **2019**, *31*, e1901404.
[6] Y. Wada, S. Kubo, H. Kaji, *Adv. Mater.* **2018**, *30*, 1705641.
[7] T. Wu, M. Huang, C. Lin, P. Huang, T. Chou, R. Chen-Cheng, H. Lin, R. Liu, C. Cheng, *Nat. Photon.* **2018**, *12*, 235.
[8] C. Chan, L. Cui, J. U. Kim, H. Nakanotani, C. Adachi, *Adv. Funct. Mater.* **2018**, *28*, 1706023.
[9] H. Park, S. H. Han, J. Y. Lee, H. Han, E. Kim, *Chem. Mater.* **2018**, *30*, 3215.
[10] T. Ohsawa, H. Sasabe, T. Watanabe, K. Nakao, R. Komatsu, Y. Hayashi, Y. Hayasaka, J. Kido, *Adv. Opt. Mater.* **2019**, *7*, 1801282.
[11] T. Lin, T. Chatterjee, W. Tsai, W. Lee, M. Wu, M. Jiao, K. Pan, C. Yi, C. Chung, K. Wong, C. Wu, *Adv. Mater.* **2016**, *28*, 6976.
[12] W. Zeng, H. Lai, W. Lee, M. Jiao, Y. Shiu, C. Zhong, S. Gong, T. Zhou, G. Xie, M. Sarma, K. Wong, C. Wu, C. Yang, *Adv. Mater.* **2018**, *30*, 1704961.
[13] R. Furue, K. Matsuo, Y. Ashikari, H. Ooka, N. Amanokura, T. Yasuda, *Adv. Opt. Mater.* **2018**, *6*, 1701147.
[14] F. M. Xie, H. Z. Li, G. L Dai, Y. Q. Li, T. Cheng, M. Xie, J. X. Tang, X. Zhao, *ACS Appl. Mater. Interfaces* **2019**, *11*, 26144.
[15] R. Pashazadeh, P. Pander, A. Lazauskas, F. B. Dias, J. V. Grazulevicius, *J. Phys. Chem. Lett.* **2018**, *9*, 1172.
[16] J. Li, R. Zhang, Z. Wang, B. Zhao, J. Xie, F. Zhang, H. Wang, K. Guo, *Adv. Opt. Mater.* **2018**, *6*, 1701256.
[17] X. Liang, Z. L. Tu, X. X. Zheng, *Chem. - Eur. J.* **2019**, *25*, 5623.
[18] D. Zhang, K. Suzuki, X. Song, Y. Wada, S. Kubo, L. Duan, H. Kaji, *ACS Appl. Mater. Interfaces* **2019**, *11*, 7192.
[19] S. Woo, Y. Kim, S. Kwon, Y. Kim, J. Kim, *ACS Appl. Mater. Interfaces* **2019**, *11*, 7199.
[20] C. Li, R. Duan, B. Li, G. Han, S. Wang, K. Ye, Y. Liu, Y. Yi, Y. Wang, *Angew. Chem. Int. Ed.* **2017**, *56*, 11525.
[21] Y. Liu, C. Li, Z. Ren, S. Yan, M. R. Bryce, *Nat. Rev. Mater.* **2018**, *3*, 18020.
[22] P. L. Dos Santos, J. S. Ward, D. G. Congrave, A. S. Batsanov, J. Eng, J. E. Stacey, T. J. Penfold, A. P. Monkman, M. R. Bryce, *Adv. Sci.* **2018**, *5*, 1700989.
[23] J. Kim, T. Batagoda, J. Lee, D. Sylvinson, K. Ding, P. G. Saris, U. Kaipa, I. W. H. Oswald, M. A. Omary, M. E. Thompson, S. R. Forrest, *Adv. Mater.* **2019**, *31*, 1900921.
[24] L. Yu, Z. Wu, G. Xie, W. Zeng, D. Ma, C. Yang, *Chem. Sci.* **2018**, *9*, 1385.
[25] S. Wang, X. Yan, Z. Cheng, H. Zhang, Y. Liu, Y. Wang, *Angew. Chem. Int. Ed.* **2015**, *54*, 13068.
[26] J. S. Ward, R. S. Nobuyasu, M. A. Fox, A. S. Batsanov, J. Santos, F. B. Dias, M. R. Bryce, *J. Org. Chem.* **2018**, *83*, 14431.
[27] K. Goushi, K. Yoshida, K. Sato, C. Adachi, *Nat. Photon.* **2012**, *6*, 253.
[28] Z. Wang, Y. Li, X. Cai, D. Chen, G. Xie, K. Liu, Y. Wu, C. Lo, A. Lien, Y. Cao, S. Su, *ACS Appl. Mater. Interfaces* **2016**, *8*, 8627.
[29] Y. Im, M. Kim, Y. J. Cho, J. Seo, K. S. Yook, J. Y. Lee, *Chem. Mater.* **2017**, *29*, 1946.
[30] Q. Zhang, H. Kuwabara, W. J. Potscavage, S. Huang, Y. Hatae, T. Shibata, C. Adachi, *J. Am. Chem. Soc.* **2014**, *136*, 18070.
[31] M. Okazaki, Y. Takeda, P. Data, P. Pander, H. Higginbotham, A. P. Monkman, S. Minakata, *Chem. Sci.* **2017**, *8*, 2677.
[32] S. Wang, Z. Cheng, X. Song, X. Yan, K. Ye, Y. Liu, G. Yang, Y. Wang, *ACS Appl. Mater. Interfaces* **2017**, *9*, 9892.
[33] J. H. Kim, J. H. Yun, J. Y. Lee, *Adv. Opt. Mater.* **2018**, *6*, 1800255.
[34] J. Li, T. Nakagawa, J. MacDonald, Q. Zhang, H. Nomura, H. Miyazaki, C. Adachi, *Adv. Mater.* **2013**, *25*, 3319.
[35] P. Data, P. Pander, M. Okazaki, Y. Takeda, S. Minakata, A. P. Monkman, *Angew. Chem. Int. Ed.* **2016**, *128*, 5833.
[36] W. Zeng, H. Lai, W. Lee, M. Jiao, Y. Shiu, C. Zhong, S. Gong, T. Zhou, G. Xie, M. Sarma, K. Wong, C. Wu, C. Yang, *Adv. Mater.* **2017**, *30*, 1704961.

